High CO_2 and CO conversion to hydrocarbons using bridged Fe nanoparticles on carbon nanotubes

Justin P. O'Byrne,[a,b] Rhodri E. Owen,[a] Daniel R. Minett,[c] Sofia I. Pascu,[a] Pawel Plucinski,[b] Matthew D. Jones,[a,*] and Davide Mattia.[b,*]

An aerosol assisted chemical vapour deposition method has been used to generate a carbon nanotube (CNT) based iron catalyst for the conversion of CO and CO_2 to longer chain hydrocarbons. The same formed iron nanoparticles (NPs) used to catalyse the growth of the CNTs were activated in-line to act as catalysts for the CO and CO_2 reduction. This methodology negates the multiple steps associated with the purification and subsequent tethering of metal catalyst nanoparticles to CNT supports common in the literature. Results show superior CO and CO_2 conversion and selectivity to higher-order hydrocarbons when compared with a traditional system where iron NPs have been deposited onto CNTs from a solution.

1. Introduction

In the context of the debate about global warming and its effects, carbon capture and storage (CCS) is currently being promoted as one of the most promising solutions to prevent further CO_2 emission into the atmosphere from power plants and industry.[1] Simply storing CO_2, though, locks a potentially large-scale feedstock for the chemical industry, one that is alternative to fossil fuels and, for now, free.[2] This advantage is at the basis of the development of the Fischer-Tropsch (FT) process for the conversion of CO and hydrogen into liquid hydrocarbons known since the 1920s,[3] using iron or cobalt catalysts.[3a, 4] The historically low cost of crude oil and its by-products meant that FT chemistry has not been exploited fully. Recent publications, though, have shown that the efficiency of converting CO to hydrocarbons can be increased significantly and be commercially competitive at current oil prices.[3b, 4b, 5] A CO/H_2 mixture flowing at high pressure over a carbon nanotube catalyst has been shown to be efficient for hydrocarbon conversion.[5a] High oil prices combined with the significant costs associated with retrofitting existing plants to capture carbon emissions open the opportunity for CO_2 to become a commercially viable feedstock for hydrocarbon production.[6]

Carbon nanomaterials provide an excellent framework for catalyst support for heterogeneous catalysis,[7] showing good adhesion for metal particles,[8] stability at elevated temperatures,[9] and relative chemical inertness.[10] Carbon-based catalysts, including carbon nanotubes, have been used for Fischer-Tropsch catalysis in the past.[3b, 5b, 11] Recently, carbon based catalysts have been used to form C_2+ hydrocarbons with good selectivity.[5a] Metal particles deposited on carbon nanotubes exhibit different behaviours over flat non-nanotube carbon supports due to the well graphitized and more strained nature of the curved support.[12] Bridged nanoparticles on supports have been shown to exhibit superior hydrogen spill-over than non-bridged equivalents.[13] Bridging occurs where there is a physical pathway for hydrogen to travel from the NP to the support surface. This bridging is important in stabilising the hydrogen after interaction with the nanoparticle during transit to the surface of the nanotube support.[13a] If a physical bridge is not present, this inhibits the transport of the resultant hydrogen species from the nanoparticle to the support surface. In the case of poor transfer from the nanoparticle to the surface, the substrates' intrinsic ability to support hydrogen species is negated. Any decrease in hydrogen spillover means there is less hydrogen on the surface of the nanotube which in turn inhibits the ability of the catalyst to reduce CO or CO_2 during the reaction.

In this work, a novel process of forming catalyst nanoparticles on the surface of multi-walled carbon nanotubes (MWNT) in a single step has been developed. The iron nanoparticles formed when catalysing CNT growth also form discrete particles on the surface of the CNTs which have been used for CO_2 and CO reduction. These particles are more active than analogous iron particles deposited on the surface of purified nanotubes. This activity difference is due to an increased interaction between the formed particles and the surface on the nanotubes of the *as-grown* Fe@CNTs over the iron deposited in CNTs *ex-situ* (Fe decorated CNTs). The increased interaction means the spillover of hydrogen from the nanoparticles onto the carbon surface is also greater, leading to a more potent catalyst with respect to classical heterogeneous systems. This work is focused on generating more active and efficient catalysts for CO_2 and CO reduction.

2. Experimental

2.1 Fe@CNT synthesis procedure

CNTs were generated by an aerosol based chemical vapour

deposition of ferrocene (0.2 g) dissolved in toluene (10 ml).[14] The ferrocene / toluene solution was injected using a syringe pump at a rate of 10 ml/hr under 450 sccm Ar and 50 sccm H_2 into a quartz tube at 790 ºC. CNTs were grown on a quartz substrate and scraped off to afford the catalyst powder. To remove the graphitised layers from the iron nanoparticles, the sample was exposed to air at 570 °C for 40 minutes in line. Before the catalyst run, the catalyst was reduced under a H_2 atmosphere.

2.2 Fe decorated CNTs

Firstly, the generated CNTs using the same aerosol cCVD growth method used to grow the Fe@CNTs were purified by being dispersed in 10 M HCl and sonicated for 1 hour followed by stirring for 24 hours.[15] The resultant solution was then filtered and the solid washed until the washings were pH neutral. The solid was then re-dispersed in 6 M HNO_3 followed by sonication for 1 hour and stirred for 24 hours to oxidise the surface of the nanotubes,[16] again the solid washed until the filtrate was pH neutral. Finally, the solid was dispersed in toluene which was mixed with an iron nanoparticle (Sigma-Aldrich) solution, this mixture was sonicated for 30 minutes and left stirring for 48 hours. The resultant solution was gently heated to remove the toluene under stirring. The resultant black slurry was heated to 270 ºC to dry for 1 hour.[17]

2.3 Analysis

TEM was carried out on a JEOL 1200 operated at 200 kV, HRTEM imaging was carried out on a JEOL 2100 (LaB6 filament) instrument operated at 200 kV. Samples for TEM analysis were prepared in ethanol and deposited onto Cu or Ni grids. SEM was carried out on a JEOL 6480LV at 5 - 25 kV. Energy-dispersive X-ray spectroscopy (EDS) was carried out in-situ during SEM analysis. The concentration of iron on the surface was calculated using the average of 5 area scans using SEM/EDS and confirmed using X-ray photoelectron spectroscopy (XPS). XPS analysis was carried out on a Kratos AXIS 165 spectrometer with the following parameters: Sample Temperature: 20-30 ºC. X-Ray Gun: mono Al K 1486.58 eV; 150 W (10 mA, 15 kV), Pass Energy: 160 eV for survey spectra and 20 eV for narrow regions. Step: 1 eV (survey), 0.05 eV (regions), dwell: 50 ms (survey), 100 ms (regions), sweeps: survey (~ 4), narrow regions (5-45). Calibration: the C 1s line at 284.8 eV was used as charge reference. Other: spectra were collected in the normal to the surface. Data processing: Construction and peak fitting of synthetic peaks in narrow region spectra used a Shirely type background and the synthetic peaks were of a mixed Gaussian-Lorenzian type. Relative sensitivity factors used are from CasaXPS library containing Scofield cross-sections. Thermogravimetric Analysis (TGA) of carbon nanotubes was collected on a Mettler Toledo TGA/DSC 1 thermogravimetric analysed over a temperature range from 20 to 900 °C at a heating rate of 10 °C min-1 under an air flow of ca. 25 ml min-1. Samples were held at 900 °C for 40 min to ensure full burn-off of all carbons. Raman spectroscopy was carried out on a Renishaw inVia at a laser wavelength of 532 nm.

2.4 Catalyst testing

Each iron-based catalyst was loaded into a purpose built stainless steel packed-bed reactor (1/2" diameter × 12 cm length) that can be heated to a variety of temperatures. The catalyst (masses in Table 1) was reduced under a pure flow of H_2 50 sccm at 400 ºC for 3 hours under atmospheric pressure. For typical carbon dioxide based experiments, CO_2 (2 sccm) and H_2 (6 sccm) were flowed over the catalysts (typically at 370 ºC). In a typical CO based experiment, CO (2 sccm) and H_2 (4 sccm) were flowed over catalysts at 300 - 390 ºC (typically 370 ºC).

2.5 Gas chromatography mass spectrometry

The product gases were analysed using GC-MS. Gas samples were taken from the exhaust gases of the reactor. Typically 30 ml of gas was sampled using a gas syringe and injected into an Agilent 7890A GCMS with a HP-PLOT/Q, 30 m long 0.530 mm diameter column. The GC-MS was calibrated with a BOC special gas with each gas composition 1 % v/v CH_4, C_2H_6, C_3H_6, C_3H_8, C_4H_{10}, CO, CO_2, with N_2 makeup gas. The carbon mass balance was carried out by the following method: The total volume and composition of the injected gases was calculated per hour. The composition of the outlet gases was analysed using GC-MS and the molar composition was calculated from the peak area and response factors calculated from the calibration gases. In all cases the mass balance was found to be satisfactory and within the range of experimental error.

3. Results and Discussion

3.1 Fe@CNT

Iron nanoparticles ranging in size from 20-60 nm as seen from TEM analysis were formed during the growth of carbon nanotubes using an aerosol based chemical vapour deposition technique Fig. 1.[14a] Fig. 1a and 1b show the formation of well graphitized carbon nanotubes with iron nanoparticles on their surface. As iron particles are formed on the surface of the tubes during growth, they exhibit a well-defined graphitic coating Fig. 1c. Fig. 1d shows a HRTEM micrograph of a highly crystalline iron particle on the surface of a CNT encapsulated by graphitic layers.

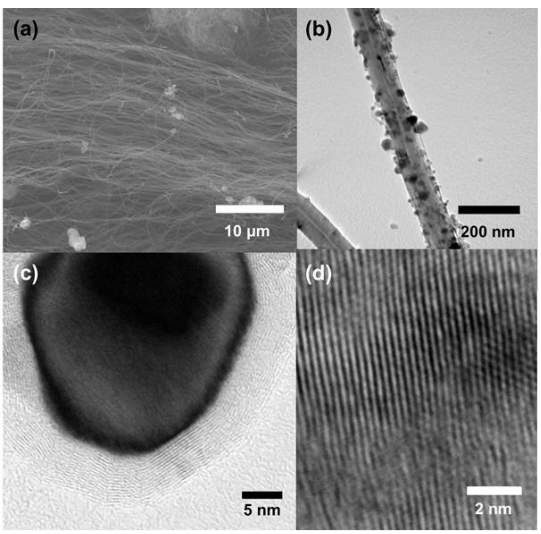

Fig. 1 (a) SEM micrograph showing as-grown Fe@CNTs; (b) TEM micrograph showing iron nanoparticles on the surface of the carbon nanotubes, (c) graphitic layers formed on the surface of as-grown nanoparticles and (d) HRTEM of iron nanoparticle on the surface of a CNT showing atomic lattice.

X

Initially, the *as-grown* Fe@CNTs were tested for their catalytic properties (see 2.3), however, due to the graphitic coating present on the iron particles' surface, there was negligible conversion. An *in-line* thermal oxidation treatment was undertaken which stripped the more physically strained carbon layers at the nanoparticles' surface than the less physically strained carbon layers in the nanotube.[18] Fe@CNTs were heated in air at 570 ºC for 40 minutes to remove the graphitic shells.[19] Fig. 2a and 2b show NPs on CNT walls with and without carbon coating, before and after thermal treatment to remove the graphitic coating, respectively. Fig. 2b also shows that the carbon nanotube integrity is not compromised by the thermal oxidation, as confirmed by thermogravimetric analysis (TGA) and Raman spectroscopy.

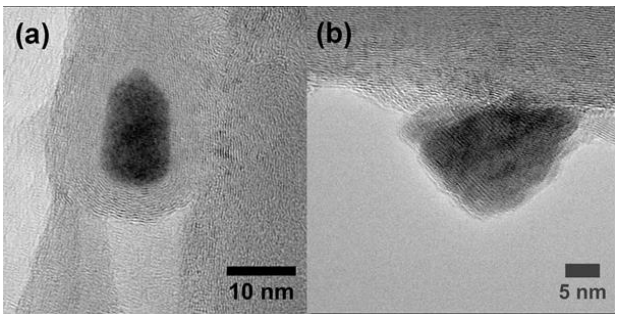

Fig.2. TEM micrographs of Fe@CNTs showing (a) an untreated, graphitic-coated, iron NP and (b) an iron nanoparticle on the CNT surface after thermal oxidation.

X-ray photoelectron spectroscopy was used to probe the iron content of Fe@CNTs at the surface of the nanotubes. The *as-grown* samples of Fe@CNTs show metallic iron present at a concentration of 0.2 atom % Fig. 3a. This low concentration is likely due to the attenuation of the signal due to the coating of the iron nanoparticles with graphitic layers Fig. 1c and Fig. 2a.[20] XPS of a thermally oxidised sample shows a clear peak for {Fe (III)} Fig. 3b. To emulate the reaction conditions and determine the active species, a sample of Fe@CNT after thermal oxidation was reduced under H_2 for 3 hours at 400 ºC. This reduced sample, analysed using XPS under air-free conditions, shows an iron concentration of ~ 1.0 atom % and the presence of mixed iron oxide {Fe(II), Fe(III)} indicated by the presence of a shoulder at 709.5 eV in addition to the principal peaks at 711.5 and 719.5 eV, Fig. 3c.[21] The Figure S2 † shows the satellite peak associated with Fe^{3+} species at 718 eV which is not obvious in the Fe^{2+} spectra.[21] Combining this information with the TEM analysis, a potential mechanism for the activation of the Fe@CNT catalysts is proposed Scheme 1. The {Fe (0)} NPs coated with graphitic layers are oxidised to {Fe (III)} during the thermal process used to remove their carbon coating. The subsequent hydrogen treatment reduces the exposed Fe nanoparticles to {Fe (II)(III)}. Therefore, the iron concentration increased from 0.2 atom % to 1.0 atom % is only apparent, as the former value was the result of the graphitic coating partially attenuating the iron signal. The overall low iron signal in the XPS analysis (lower that what expected given the Fe loadings in Table 1 can be attributed to the tubular nature of the catalyst support.

Iron particles are resident all over the tubes and their signal is not seen due to blocking from the nanotubes. The whole process - CNT growth, graphitic layer oxidation and reduction of the catalyst - can take place in line using the initial CNT growth temperature to heat the sample in air and then reduce it under hydrogen, significantly simplifying the preparation of the catalyst over traditional methods.[17, 22]

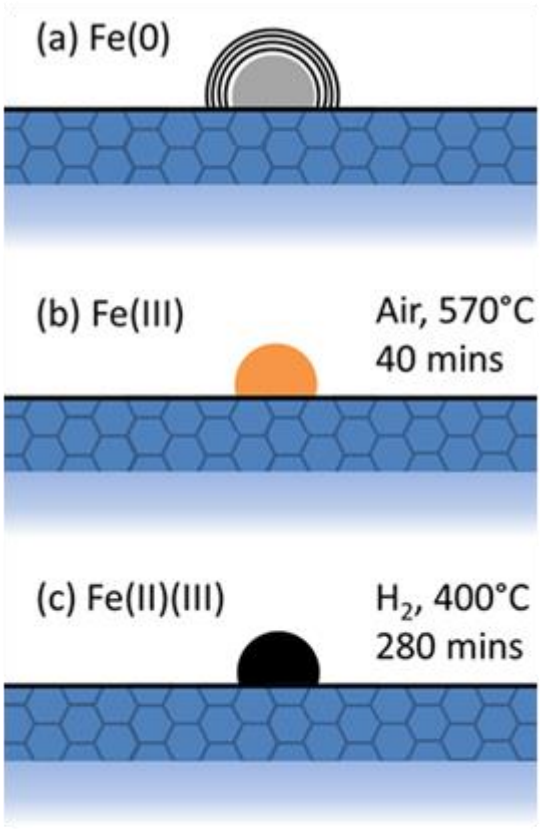

Scheme 1 Oxidation states of (a) untreated iron nanoparticle coated in graphitic carbon (not to scale), (b) thermally oxidised nanoparticle with carbon layers removed and (c) reduced particle treated with H_2

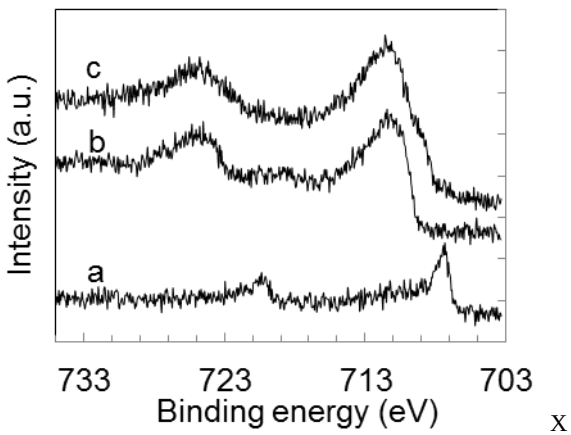

Fig.3 XPS (2p region $2p_{3/2}$ ~ 710 and $2p_{1/2}$ ~ 725 eV) analysis of the oxidation states of iron particles on the Fe@CNT catalysts (a) untreated as-grown, (b) 40 min at 570 °C oxidised in air, and (c) reduced in 50 sccm H_2 at 400 °C for 280 min.

3.2 Fe decorated CNTs

To compare the reactivity of the *active* Fe@CNT samples, iron decorated CNTs were synthesised. HRSEM Fig. 4a micrographs show the product for the iron decorated CNTs. Fig. 4b and 4c show the deposition of iron nanoparticles on the surface of the nanotubes. XPS analysis of the catalyst before reduction showed iron to be Fe(III), and the loading to be ~ 1 atom %. The XPS and SEM/EDS gave matching loadings of Fe on the surface of the CNTs. These techniques were used to accurately assess Fe loading. Whereas the XPS analysis was taken in a single spot, SEM/EDS was used to gain an average over 5 scans on the surface of the Fe decorated CNTs to give an accurate iron loading.

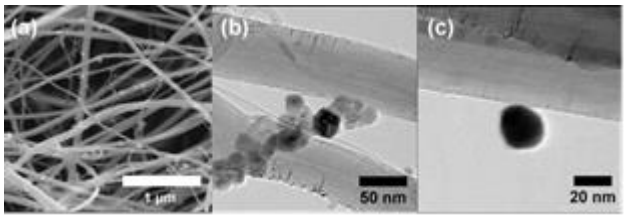

Fig.4 (a) SEM micrograph of Fe decorated CNTs and (b) and (c) TEM micrographs showing iron nanoparticles deposited on the surface of CNTs.

3.3 Catalytic results

Table 1 Catalyst loading in the reactor with the iron loading on the CNT surface and the normalised iron content per reaction. The variation in the masses of the catalyst loading is due to the differences in the densities of each catalyst

Catalyst	Iron (%) loading on surface	Typical catalyst loading (g)[a]	Iron loading per run (g)
Fe@CNT	1.1	0.4	0.004
Fe decorated CNT	1.3	0.7	0.009

[a] Mass of catalyst needed to pack entire length of reactor

Table 1 shows the effective loadings of iron on each of the supports. XPS analysis coupled with SEM/EDS was used to calculate the iron loading on the surface of the supports. Thermogravimetric analysis (TGA) was taken into consideration during iron loading analysis, however due to the presence of inaccessible iron in the core of the nanotubes skewing the effective loading, XPS and EDS was used. The iron time yield (FTY) is reported to normalise the conversion and activity of each catalyst Tables 2 and 3, following the method reported by Torres Galvis *et al*.[5a] The FTY is defined as number of mol of CO or CO_2 reduced to products divided by grams of iron catalyst per second. The amount of iron per catalyst is calculated to find the effective difference in catalyst loading *in lieu* of mass of catalyst used per test. The mass of catalyst used varies to maintain the same volume of the packed bed, as the densities of the supports are significantly different Table 1. The conversion of CO to hydrocarbons and the iron time yield numbers from each of the Fe on CNT catalysts is shown in Table 2. *Active* Fe@CNT was a more effective catalyst than the analogous iron nanoparticles decorated on CNTs (Tables 2 and 3). The FTY_{CO} {iron time yield (mol CO converted to hydrocarbons / grams of iron used per second)} of both Fe@CNT and Fe decorated CNTs was found to be one order of magnitude greater (FTY_{CO} 1.41×10^{-6} mol /g s) at ambient pressure, with similar conversions at 20 bar than the best iron-carbon catalyst reported in the literature, albeit with slightly lower selectivity towards C_2+ hydrocarbons (~57 %).[5a]

Table 2 Conversion of CO and selectivity. The iron time yield is reported as the conversion of CO to hydrocarbons per grams of iron per second (molCO/gFe s). The reactions are undertaken at atmospheric pressure and at a temperature of 370 ºC

Catalyst	FTY (10^{-5}) mol/g s	C1	C2-4	C5+
Fe@CNT	9.4	43.3	54.4	2.3
Fe decorated CNT	6.0	41.6	53.6	4.5

Table 3 Conversion of CO_2 and selectivity. The FTY is reported as conversion of CO_2 per grams of iron per second ($molCO_2$/gFe s). The reactions are undertaken at atmospheric pressure and at a temperature of 370 ºC.)

Catalyst	FTY (10^{-5}) mol/g s	CO	C1	C2-4	C5+
Fe@CNT	11	45.1	29.3	24.3	1.3
Fe decorated CNT	3.0	82.4	12.4	5.2	0

While the conversion of CO to hydrocarbons is the most studied and most efficient process, a direct conversion of carbon dioxide to hydrocarbons has more potential for industrial applications as it would eliminate the CO_2 to CO preliminary step. As expected, direct conversion of CO_2 using the *active* Fe@CNT yielded only 55% selectivity towards hydrocarbons, with the remainder being CO (Table 3). Despite the lower selectivity, the high FTY_{CO2} value for the active Fe@CNT catalyst means that this process can still be commercially viable if the produced CO is recycled in the reactor as an active feedstock. The Fe@CNT was tested over a 65 hour period and the FTY_{CO2} decreased by approximately 20 % in the first 12 hours but stabilised over the remainder of the 65 hour period. Fe@CNT catalyst was also regenerated 5+ times with no discernible loss from the initial catalytic activity. Fe@CNT was a more superior catalyst with respect to the Fe-decorated CNTs for both selectivity to longer chain hydrocarbon formation from CO_2 and conversion percentages as shown in Table 3. Both Fe@CNT and Fe decorated CNTs were tested at atmospheric pressure.

3.4 Behind the catalysis

Carbon based materials exhibit superior hydrogen support from spillover from nanoparticles than silica based alternatives.[23] Greater hydrogen spillover can yield more feedstock hydrogen being available from the surface of the nanotube during CO/CO_2 reduction leading to greater reactivity.[24] Fig. 2b shows the differences between the catalyst particles formed on Fe@CNT and catalyst particles deposited on the surface of the CNTs (Fe decorated CNTs) Fig. 4b and 4c. As a result of the synthesis process, the iron nanoparticles in Fe@CNT have a significantly larger contact area with the nanotubes' surface than the NPs linked to the surface only by a covalent tether (*cf.* Fig. 2b and 4c). As the iron interaction with the CNTs' surface in Fe@CNT is greater than Fe decorated CNTs, Fe@CNT is more able to dissociate H_2 on the iron surface and stabilise the resultant species on the surface of the nanotube.[13a] Iron particles deposited on the surface of CNTs during the CNT growth phase mould to

the NT's surface Fig. 3b. This *in-situ* deposition ensures a pyramidal nanoparticle shape, ideal as a bridged pathway from NP tip to CNT surface.[13b]

Statistical image analysis of TEM micrographs for the two systems showed that average particle sizes are compatible, with values of 39±14 and 31±12 nm for the Fe decorated CNTs and the Fe@CNTs, respectively (at least 30 particles for each system were measured, see Supporting Information Figure S4, S5 and S6). Whilst it has been observed in the literature that particle size can have an effect on reactivity, the difference in size is too small to affect the catalysis meaningfully.[25] This conclusion is corroborated by the close selectivity values for the two catalysts in the CO/H_2 process. On the other hand, the almost four-fold increase in conversion for the CO_2/H_2 can be explained by the much stronger hydrogen spillover effect in the Fe@CNT system.[23d]

Oxidised graphitic structures have been reported to be able to stabilise hydrogen on their surface more efficiently than non-oxidised graphitic structures.[26] The energy barrier for the migration of hydrogen from a hydroxyl group to an adjacent epoxide oxygen is lower than the energy barrier for the migration of a hydrogen atom across a graphite surface.[26] XPS analysis of the surface of the carbon nanotubes shows the existence of various oxygenated species on the surface of the nanotube catalyst.† C-O-C, C-OH, C=O, O-C=O functional groups are present in concentrations of around 16 atom % of the total carbon species of the untreated and oxidised nanotubes to approximately 14 atom % of the total carbon species in the reduced/active Fe@CNTs. TGA and Raman also confirm the presence of well graphitized nanotubes before and after oxidation.

4. Conclusions

Two iron catalysts have been used to form hydrocarbons from CO_2 and CO. Iron nanoparticles deposited on carbon nanotubes have been grown *in-situ* during CNT growth and used for the reduction of CO and CO_2. To compare the activity of the nanoparticles grown *in situ*, nanoparticles were deposited on purified CNTs. The carbon nanotube/iron catalyst (Fe@CNT) is more catalytically active than analogous iron nanoparticles deposited on CNTs *ex-situ*. To the best of the authors' knowledge, FTY of ~10^{-4} mol/(g s) and ~57% conversion to C_2+ hydrocarbons achieved for CO hereby showed a significant improvement over the most active carbon / Fe catalysts reported thus far.[5a] The increased activity is attributed to the propensity of the Fe@CNT particles to more efficiently load the support surface around the catalyst particle with hydrogen to feed the CO/CO_2 reduction, due to a large contact area between the NP and the tube's surface. Work is on-going to probe the interactions between H_2 and the nanoparticle in more detail.

Acknowledgements

The authors wish to acknowledge EPSRC (EP/H046305/1), the Centre for Sustainable Chemical Technologies (CSCT) and Bath Ventures at University of Bath for funding. SIP wishes to thank the Royal Society for funding. The authors would also like to acknowledge the use of facilities at the Research Complex at Harwell and the MAS Centre at Bath.

Notes

[a] *Department of Chemistry, University of Bath, Claverton Down, Bath BA2 7AY, UK. Fax: +44 (0) 1225 386231 Tel: +44 (0) 1225 384908; E-mail: mj205@bath.ac.uk*

[b] *Department of Chemical Engineering, University of Bath, Claverton Down, Bath BA2 7AY, UK.*

[c] *Doctoral Training Centre in Sustainable Chemical Technologies, University of Bath, Bath, BA2 7AY (UK)*

† Electronic Supplementary Information (ESI) available: [details of any supplementary information available should be included here]. See DOI: 10.1039/b000000x/

References

1. G. Wong-Parodi, H. Dowlatabadi, T. McDaniels and I. Ray, *Environ. Sci. Technol.*, 2011, **45**, 6743-6751.
2. G. Centi, G. Iaquaniello and S. Perathoner, *ChemSusChem*, 2011, **4**, 1265-1273.
3. (a) H. Schulz, *Appl. Catal. A*, 1999, **186**, 3-12; (b) G. L. Bezemer, J. H. Bitter, H. P. C. E. Kuipers, H. Oosterbeek, J. E. Holewijn, A. J. van Dillen and K. P. de Jong, *J. Am. Chem. Soc.*, 2006, **128**, 3956-3964; (c) E. de Smit and B. M. Weckhuysen, *Chem. Soc. Rev.*, 2008, **37**, 2758-2781; (d) C. K. Rofer-DePoorter, *Chem. Rev.*, 1981, **81**, 447-474; (e) D. A.K.; and B. H. Davis, *Applied Catalysis A: General*, 2008, **348**, 1-15; (f) V. U. S. Rao, G. J. Stiegel, G. J. Cinquegrane and R. D. Srivastava, *Fuel Processing Technology*, 1992, **30**, 83-107; (g) E. Iglesia, *Applied Catalysis A: General*, 1997, **161**, 59-78; (h) V. R. Calderone, N. R. Shiju, D. C. Ferré and G. Rothenberg, *Green Chemistry*, 2011, **13**, 1950-1959; (i) W. Wang, S. Wang, X. Ma and J. Gong, *Chem Soc Rev*, 2011, **40**, 3703-3727.
4. (a) D. Leckel, *Energy Fuels*, 2009, **23**, 2342-2358; (b) A. Y. Khodakov, W. Chu and P. Fongarland, *Chem. Rev.*, 2007, **107**, 1692-1744.
5. (a) H. M. Torres Galvis, J. H. Bitter, C. B. Khare, M. Ruitenbeek, A. I. Dugulan and K. P. de Jong, *Science*, 2012, **335**, 835-838; (b) Y. Zhu, Y. Ye, S. Zhang, M. E. Leong and F. Tao, *Langmuir*, 2012, **28**, 8275-8280.
6. (a) P. T. Anastas and M. M. Kirchhoff, *Accounts of Chemical Research*, 2002, **35**, 686-694; (b) M. Peters, B. Kohler, W. Kuckshinrichs, W. Leitner, P. Markewitz and T. E. Muller, *ChemSusChem*, 2011, **4**, 1216-1240; (c) K. M. K. Yu, I. Curcic, J. Gabriel and S. C. E. Tsang, *ChemSusChem*, 2008, **1**, 893-899; (d) M. Aresta and A. Dibenedetto, *Dalton Trans.*, 2007, 2975-2992.
7. (a) P. Serp and J. L. Figueiredo, *J. Am. Chem. Soc.*, 2009, **131**, 9856-9857; (b) E. Antolini, *Materials Chemistry and Physics*, 2002, **78**, 562-573.
8. (a) G. G. Wildgoose, C. E. Banks and R. G. Compton, *Small*, 2006, **2**, 182-193; (b) W. A. Solomonsz, G. A. Rance, M. Suyetin, A. La Torre, E. Bichoutskaia and A. N. Khlobystov, *Chemistry - A European Journal*, 2012, **18**, 13180-13187.
9. Y. A. Kim, H. Muramatsu, T. Hayashi, M. Endo, M. Terrones and M. S. Dresselhaus, *Chem. Phys. Lett.*, 2004, **398**, 87-92.
10. F. Rodríguez-reinoso, *Carbon*, 1998, **36**, 159-175.
11. (a) H. J. Schulte, B. Graf, W. Xia and M. Muhler, *ChemCatChem*, 2012, **4**, 350-355; (b) R. M. Malek Abbaslou, J. Soltan and A. K. Dalai, *Applied Catalysis A: General*, 2010, **379**, 129-134; (c) R. M. Malek Abbaslou, A. Tavasoli, J. Soltan and A. K. Dalai, *Applied Catalysis A: General*, 2009, **367**, 47-52; (d) M. C. Bahome, L. L.

Jewell, D. Hildebrandt, D. Glasser and N. J. Coville, *Applied Catalysis A: General*, 2005, **287**, 60-67.
12. Y. Zhang, N. W. Franklin, R. J. Chen and H. Dai, *Chem. Phys. Lett.*, 2000, **331**, 35-41.
13. (a) A. J. Lachawiec, G. Qi and R. T. Yang, *Langmuir*, 2005, **21**, 11418-11424; (b) Y. Li and R. T. Yang, *J. Am. Chem. Soc.*, 2006, **128**, 8136-8137.
14. (a) C. Singh, M. S. P. Shaffer and A. H. Windle, *Carbon*, 2003, **41**, 359-368; (b) D. R. Minett, J. P. O'Byrne, M. D. Jones, V. P. Ting, T. J. Mays and D. Mattia, *Carbon*, 2013, **51**, 327-334.
15. J.-M. Moon, K. H. An, Y. H. Lee, T. S. Park, D. J. Bae and G.-S. Park, *J. Phys. Chem. B*, 2001, **105**, 5677-5681.
16. I. D. Rosca, F. Watari, M. Uo and T. Akasaka, *Carbon*, 2005, **43**, 3124-3131.
17. V. Georgakilas, D. Gournis, V. Tzitzios, L. Pasquato, D. M. Guldi and M. Prato, *J. Mater. Chem.*, 2007, **17**, 2679-2694.
18. K. Min Lee, L. Li and L. Dai, *J. Am. Chem. Soc.*, 2005, **127**, 4122-4123.
19. E. Flahaut, F. Agnoli, J. Sloan, C. O'Connor and M. L. H. Green, *Chem. Mater.*, 2002, **14**, 2553-2558.
20. D. Briggs and J. T. Grand, *IMPublications, Chichester, UK and SurfaceSpectra*, 2003.
21. T. Yamashita and P. Hayes, *Applied Surface Science*, 2008, **254**, 2441-2449.
22. (a) Y. Lin, K. A. Watson, M. J. Fallbach, S. Ghose, J. G. Smith Jr, D. M. Delozier, W. Cao, R. E. Crooks and J. W. Connell, *ASC Nano*, 2009, **3**, 871-884; (b) X. R. Ye, Y. Lin and C. M. Wai, *Chem. Commun.*, 2003, 642-643.
23. (a) L. Wang and R. T. Yang, *Catalysis Reviews: Science and Engineering*, 2010, **52**, 411-461; (b) C. H. Chen and C. C. Huang, *Microporous and Mesoporous Materials*, 2008, **109**, 549-559; (c) X. Dong, H. B. Zhang, G. D. Lin, Y. Z. Yuan and K. R. Tsai, *Catalysis Letters*, 2003, **85**, 237-246; (d) R. Prins, *Chem. Rev.*, 2012, **112**, 2714-2738; (e) F. H. Yang, A. J. Lachawiec and R. T. Yang, *J. Phys. Chem. B*, 2006, **110**, 6236-6244.
24. (a) G. F. Taylor, S. J. Thomson and G. Webb, *J. Catal.*, 1968, **12**, 191-197; (b) S. T. Srinivas and P. K. Rao, *J. Catal.*, 1994, **148**, 470-477.
25. (a) V. K. Jones, L. R. Neubauer and C. H. Bartholomew, *J. Phys. Chem.*, 1986, **90**, 4832-4839; (b) J. Y. Park, Y. J. Lee, P. K. Khanna, K. W. Jun, J. W. Bae and Y. H. Kim, *Journal of Molecular Catalysis A: Chemical*, 2010, **323**, 84-90; (c) H. M. Torres Galvis, J. H. Bitter, T. Davidian, M. Ruitenbeek, D. A.I.; and K. P. de Jong, *J. Am. Chem. Soc.*, 2012, **134**, 16207-16215.
26. G. M. Psofogiannakis and G. E. Froudakis, *J. Am. Chem. Soc.*, 2009, **131**, 15133-15135.

